



Article

On Numerical Models for Cube Drop Test of Bladder Fuel Tank for Aeronautical Applications

Domenico Cristillo ¹, Francesco Di Caprio ^{1,*} , Claudio Pezzella ², Carmen Paciello ², Simone Magistro ³, Luigi Di Palma ⁴  and Marika Belardo ¹

- ¹ CIRA—Italian Aerospace Research Centre, Via Maiorise, 81043 Capua, CE, Italy; d.cristillo@cira.it (D.C.); m.belardo@cira.it (M.B.)
- ² Step Sud Mare SRL, Via Ex Aeroporto c/o Consorzio Il Sole, LOTTO X1, 80038 Pomigliano d'Arco, NA, Italy; claudio.pezzella@stepsudmare.com (C.P.); carmen.paciello@stepsudmare.com (C.P.)
- ³ Aero Secur S.p.a., Via Delle Valli 46, 04011 Aprilia, LT, Italy; simone.magistro@secur.aero
- ⁴ Maregroup, Via Ex Aeroporto c/o Consorzio Il Sole, LOTTO X1, 80038 Pomigliano d'Arco, NA, Italy; luigi.dipalma@maregroup.it
- * Correspondence: f.dicaprio@cira.it; Tel.: +39-082-362-3538

Abstract: For some categories of aircraft, such as helicopters and tiltrotors, fuel storage systems must satisfy challenging crash resistance requirements in order to reduce or eliminate the possibility of fuel fires and thus increase the chances of passenger survival. Therefore, for such applications, fuel tanks with high flexibility (bladder) are increasingly used, which are able to withstand catastrophic events and avoid fuel leakages. The verification of these capabilities must be demonstrated by means of experimental tests, such as the cube drop test (MIL-DTL-27422). In order to reduce development costs, it is necessary to execute experimental tests with a high confidence of success, and, therefore, it is essential to have reliable and robust numerical analysis methodologies. The present work aims to provide a comparison between two explicit FE codes (i.e., Abaqus and Ls-Dyna), which are the most frequently used for such applications according to experimental data in the literature. Both codes offer different material models suitable for simulating the tank structure, and therefore, the most suitable one must be selected by means of a specific trade-off and calibration activity. Both are able to accurately simulate the complex fluid–structure interaction thanks to the use of the SPH approach, even if the resulting sloshing capabilities are quite different from each other. Additionally, the evolution of the tank's deformed shape highlights some differences, and, in particular, Abaqus seems to return a more natural and less artificial behavior. For both codes, the error in terms of maximum impact force is less than 5%, but, even in this case, Abaqus is able to return slightly more accurate results.

Keywords: SPH; hyperelastic; drop test; fuel tank; FEM; explicit analysis; bladder; tiltrotor



Citation: Cristillo, D.; Di Caprio, F.; Pezzella, C.; Paciello, C.; Magistro, S.; Di Palma, L.; Belardo, M. On Numerical Models for Cube Drop Test of Bladder Fuel Tank for Aeronautical Applications. *J. Compos. Sci.* **2022**, *6*, 99. <https://doi.org/10.3390/jcs6030099>

Academic Editor: Stelios K. Georgantzinou

Received: 14 February 2022

Accepted: 18 March 2022

Published: 21 March 2022

Publisher's Note: MDPI stays neutral with regard to jurisdictional claims in published maps and institutional affiliations.



Copyright: © 2022 by the authors. Licensee MDPI, Basel, Switzerland. This article is an open access article distributed under the terms and conditions of the Creative Commons Attribution (CC BY) license (<https://creativecommons.org/licenses/by/4.0/>).

1. Introduction

The runway-independent aircraft concept is progressively becoming more prominent in civil aviation thanks to its ability to improve public mobility in areas where airport infrastructures are not highly developed. Horizon 2020 Clean Sky 2 FRC IADP Next Generation of Civil Tiltrotor Technology Demonstrator (NGCTR-TD) is an example of European-funded research in the sector of VTOL aircraft. NGCTR-TD is the innovative Civil Tiltrotor Technology Demonstrator [1,2] with a configuration that will go beyond current architectures for this type of aircraft. NGCTR-TD is currently under development by Leonardo Helicopter (helicopter division of Leonardo Company, leader in Italian aerospace and defense), and it is shown in Figure 1.



Figure 1. NGCTR tiltrotor, courtesy of Leonardo Helicopters (<https://svppbellum.blogspot.com/2020/01/il-next-generation-civil-tiltrotor.html>, accessed on 28 January 2022).

Because the tiltrotor is able to operate as both a helicopter and an aircraft, the airworthiness specifications are a combination of CS-25 and CS-29 Airworthiness Requirements, and in some cases, specific tailoring is necessary. For their VTOL capability, tiltrotors have to comply with crashworthiness requirements according to CS-29, similarly to helicopters. The fuel storage system of the NGCTR-TD consists of bladder tanks installed inside the wing structures. Crashworthiness is one of the most demanding aspects to consider in the design of VTOL fuel tanks in order to satisfy passenger survivability requirements. Among the various requirements, tanks have to successfully pass a drop test from a height equal to 15.2 m according to CS 29.952 [3] by showing no leakage after the drop. Moreover, the tanks must possess sufficient flexibility and foldability in order to be installed through suitable access doors placed on the lower skin of the wing and to be used for inspection and maintenance activities. NGCTR-TD has 14 fuel bladder tanks, all located in the wing structure [4]. As an example, the V22 has 16 fuel tanks, 10 integrated into the wings and 6 in the fuselage, holding from 5489 to 13,779 L of fuel [5]. The NCGTR-TD fuel storage system is based on bladder tanks manufactured from very flexible and resistant rubberized materials. Each tank provides a fuel barrier against fuel and fuel vapor leakages and mechanical resistance in case of a crash, puncture or penetration. All tanks are completed with co-cured metallic flanges and valves to connect the fuel storage system with fuel and venting lines.

Not only must the tanks be designed according to crashworthiness requirements, but the wing itself must have crashworthy features, such as the ability to separate itself from the fuselage to ensure that a crash is survivable. This is necessary to prevent the fuselage from being crushed due to the inertial load related to the wings, fuel and nacelles and to let passengers escape from the aircraft. This feature is also present in military tiltrotors, such as Bell V-22 tiltrotor [6]. The civil application should require an experimental test to prove the effectiveness of any solutions devoted to breaking the wing in specific sections. Experimental and numerical studies of a full-scale regional fuselage drop test without any wings installed [7–9] have demonstrated that the fuselage damage is located mainly on the lower section of the fuselage, while the upper part is not critically damaged [10,11]. No evidence on the structural behavior of the wing during a crash has been obtained under crash conditions. In the 1960s, the US Army introduced the first military regulation (MIL-DTL-27422) that defined the certification requirements for fuel storage systems to be installed in a helicopter. The crashworthiness of a tiltrotor tank is based on CS-29 and MIL-DTL-27422 specifications, similarly to a helicopter [12]. As described in MIL-DTL-27422, the drop impact test must be conducted to verify the structural behavior in a dynamic regime of the fuel tank, both in the standalone configuration (cube drop test) and in the partially integrated configuration with the surrounding structure [13]. The Federal Aviation Administration (FAA) funded research on crash-resistant fuel systems for commercial aircraft with the aim of providing data that are useful in reducing the possibility of fire due to crash events [14,15]. Anghileri [16] investigated the fuel tank crashworthiness

from experimental and numerical points of view. Fuel sloshing during crash events was studied by means of numerical models, which were validated by comparing their outputs to experimental results [17]. Using parallel computing, Li et al. [18] investigated the dynamic behavior of a fuel tank in a dynamic impact event with the ground, demonstrating that such an algorithm is able to run with a high speed-up ratio and parallel efficiency. Luo et al. [19] studied the crashworthiness of a fuel tank for helicopter applications by means of the finite element method (FEM) in order to verify the energy absorption capabilities of the textile layer and protection frame. Kim et al. [20] used the commercial FE code Ls-Dyna to simulate the dynamic response of fuel tanks installed in a rotorcraft. An accurate study based on analytical, numerical and experimental results was performed to investigate the structural performance of tanks with energy-absorbing fixtures under dynamic pressure and blast load conditions [21,22].

The activities aimed at developing the next-generation fuel storage system of NGCTR-TD are part of the DEFENDER project, and within the design and analysis work package, an innovative aspect is represented by the setup of high-fidelity methodologies and models to support the tank design, especially its performance against crash and impact loads. The final aim is to provide models that are validated by means of a full-scale crash test on the most critical tank plus the wing surrounding its composite structure. The activity will be performed with an incremental approach, which passes through numerical–experimental validation, the simulation of a cube-like tank test and, finally, a full-scale test. The study presented herein is one of the basic steps foreseen for the final objective of the high-fidelity crashworthiness simulation. In particular, in this work, two numerical models for the prediction of the structural response of a cube-like tank under impact load conditions were developed and verified by comparing their results with experimental data available in the literature.

2. Experimental Test Case Description

In order to validate the numerical model, experimental data available in the literature [23] were used. Yang et al. performed two drop tests on a fuel tank filled with water (to replace real fuel). The fuel tank was realized with a flexible structure made of an external fabric nylon layer and an inner sealing layer. The tank was 760 mm long and wide and its height is about 600 mm. In order to execute the drop test, according to the specification, the tank was filled with about 350 kg of water. In the drop impact test, the tank was lifted to a specific height by means of a crane and dropped on a rigid impact surface instrumented with four load cells with a capacity equal to 2000 kN. The impact surface was a steel plate and was 80 mm thick; therefore, it can be reasonably considered rigid. They performed two drop tests using two different drop heights: 15.2 and 19.8 m. The impact velocities related to these drop heights are 17.3 and 19.7 m/s, respectively. For the following numerical comparison, only the impact velocity equal to 17.3 m/s was taken into account, because it is related to a standard drop height, as reported in MIL-DTL-27422.

3. Numerical Model Description

The validation of the experimental test, as previously described, was performed by means of a numerical model, realized with two different software packages: Abaqus and LS Dyna. The experimental test was simulated by means of a 3D FE model composed of three parts: the fuel tank, the ground and the fuel. In particular, the fuel tank was modeled by using shell elements with a thickness of 2 mm and fuel with SPH elements, and the ground was discretized by means of rigid elements in Abaqus and a rigid wall in Ls-Dyna.

For both ABAQUS and Ls-Dyna models, the same mesh density was adopted in order to remove any dependency by the discretization technique. The tank structure was discretized by means of 31728 shell elements, while the number of smooth particle hydrodynamics (SPH) elements used for modeling the fuel was 537936. The platform used for the numerical simulations is an HP Z840 workstation, equipped with an Intel Xeon E5-2620 v3 CPU @ 2.40 GHz and 128 GB RAM. Considering that the simulated event time is

200 ms (even if the most relevant part is up to 50 ms), the computational time is about 4.5 h for Abaqus and about 4 h for Ls-Dyna (both codes run adopting the parallel solution with 4 cores). Obviously, this small difference is also related to the requested output; therefore, the difference in computational time is not too relevant. Figure 2 reports the adopted numerical model with schematic detail of SPH elements and the fluid–structure interaction.

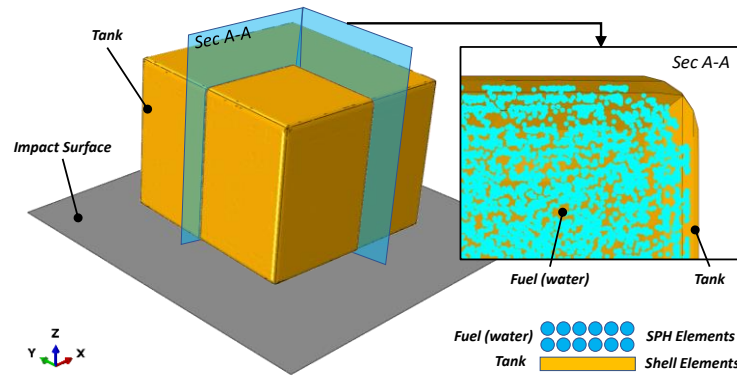


Figure 2. FE model.

3.1. Boundary Conditions

The tank is subject to a free-fall form and height equal to 15.2 m; therefore, the impact velocity is about 17.3 m/s. The ground was simulated by means of rigid elements.

Further, from the reference work, it can be assumed that the impact angle is not equal to zero, but it is worth noting that such a condition is quite hard to obtain. The impact angle is about 3° around both the X and Y axes. Figure 3 schematically reports the adopted boundary conditions.

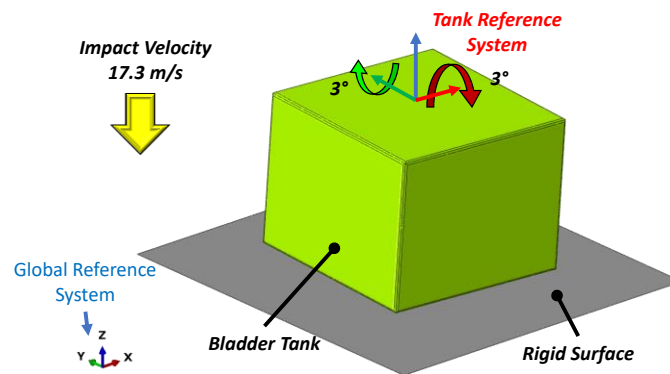


Figure 3. Boundary conditions.

3.2. Smooth Particle Hydrodynamics Method (SPH) and Water Material Model

Smoothed particle hydrodynamics (SPH) are represented by three-dimensional elements with three degrees of freedom and defined by their center of mass. These elements have their own shape functions that depend on the connectivity of the particles. The interpolation distance between the particles, called smoothing length, furnishes the location and provides information about transmission among the different particles.

In the SPH approach, the water was simulated as particles with the same dimensions and distances without mass. The velocity and energy of the particles at any time can be solved by means of a function $f(x)$. The value of this function can be approximated for particle data by Equation (1):

$$\langle f(x_i) \rangle = \sum_{j=1}^N \frac{m_j}{\rho_j} f(x_j) W(x_i - x_j, h) \tag{1}$$

where h is the smoothing length, m_i and ρ_i are the mass and density of the particle, x_i and x_j are the positions of particles, and W is the kernel interpolation.

In particular, we consider two particles (i and j) to be nearest neighbors. If the distance between particles i and j is lower than the radius of the sphere of influence of j , then i is connected to j . The dimension of the sphere of influence is a multiple of the particle's smoothing length, and the multiplication factor depends on the kernel used to create the smooth particle's shape function.

Therefore, the value of a variable for particle j can be obtained by adding the contributions of particle i contained within the influence radius. The interpolation kernel used in this analysis was proposed by Monaghan [24].

The behavior of the fluid material inside the fuel tank is determined by the equation of state (EOS), which relates the pressure and the material volume change rate in a physical state.

The equation for the conservation of energy equates the increase in internal energy per unit mass, E_m , to the rate at which work is being performed by stresses and the rate at which heat is being added. In the absence of heat conduction, the energy equation can be written as:

$$\rho \frac{\partial E_m}{\partial t} = (p - p_{bv}) \frac{1}{\rho} \frac{\partial \rho}{\partial t} + S : \dot{\epsilon} + \rho \dot{Q} \tag{2}$$

where p is the pressure stress, defined as positive in compression; p_{bv} is the pressure stress due to the bulk viscosity; S is the deviatoric stress tensor; $\dot{\epsilon}$ is the deviatoric part of the strain rate; and \dot{Q} is the heat rate per unit mass.

The equation of state is assumed for the pressure as a function of the current density, ρ , and the internal energy per unit mass, E_m .

Since the internal energy can be eliminated, it is possible to write the EOS as a p versus V relationship (where V is the current volume) or, equivalently, a p versus $1/\rho$ relationship that is unique to the material described by the equation-of-state model. This unique relationship is called the Hugoniot curve and is the locus of p - V states achievable behind a shock (see Figure 4).

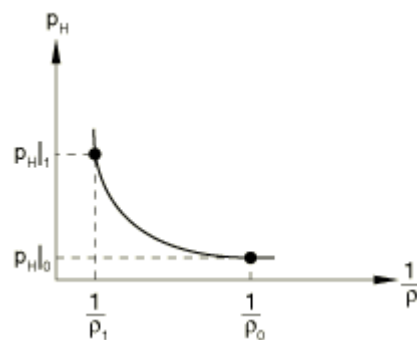


Figure 4. A schematic representation of a Hugoniot curve.

The Hugoniot pressure, p_H , is a function of density only and can be determined, in general, by fitting experimental data.

There are different formulations of EOS, and the most common form for the water description is the linear U_s - U_p equation, which is given by:

$$p_H = \frac{\rho_0 c_0^2 \eta}{(1 - s\eta)^2} \tag{3}$$

where c_0 and s define the linear relationship between the shock velocity, U_s , and the particle velocity, U_p , as follows:

$$U_s = c_0 + sU_p \tag{4}$$

With the above assumptions, the linear $Us-Up$ Hugoniot form is written as

$$p = \frac{\rho_0 c_0^2 \eta}{(1 - s\eta)^2} \left(1 - \frac{\Gamma_0 \eta}{2} \right) + \Gamma_0 \rho_0 E_m \tag{5}$$

where $\rho_0 c_0^2$ is equivalent to the elastic bulk modulus at small nominal strains.

3.3. Tank Material Model

The fuel tank structure is a crash-resistant composite fabric composed of a rubber layer and a nylon layer. A different formulation is used for each of these materials.

Rubber materials have very small compressibility compared to their shear flexibility. This behavior can be modeled by means of hyperplastic material. In fact, the hyperplastic material model is isotropic and nonlinear, is valid for materials that exhibit an instantaneous elastic response to large strains and requires that geometric nonlinearity be accounted for during the analysis step since it is intended for finite-strain applications.

Hyperelastic materials are described in terms of a “strain energy potential”, $U(\epsilon)$, which defines the strain energy stored in the material per unit of reference volume (volume in the initial configuration) as a function of the strain at that point in the material. There are several forms of strain energy potentials available in Abaqus to model approximately incompressible isotropic elastomers: the Arruda–Boyce form, the Marlow form, the Mooney–Rivlin form, the neo-Hookean form, the Ogden form, the polynomial form, the reduced polynomial form, the Yeoh form and the van der Waals form. For this material description, the Marlow form is used. A strain energy potential is constructed that will reproduce the test data exactly and that will have reasonable behavior in other deformation modes.

The form of the Marlow strain energy potential is:

$$U = U_{dev}(\bar{I}_1) + U_{vol}(J^{el}) \tag{6}$$

where U is the strain energy per unit of reference volume, with U_{dev} as its deviatoric part and U_{vol} as its volumetric part; \bar{I}_1 is the first deviatoric strain invariant and is defined as:

$$\bar{I}_1 = \bar{\lambda}_1^2 + \bar{\lambda}_2^2 + \bar{\lambda}_3^2 \tag{7}$$

where the deviatoric stretch $\bar{\lambda}_i = J^{-\frac{1}{3}} \lambda_i$ is the total volume ratio, J^{el} is the elastic volume and λ_i is the principal stretch. The deviatoric part of the potential is determined by providing either uniaxial, equibiaxial or planar test data, while the volumetric part is determined by providing the volumetric test data, defining Poisson’s ratio or specifying lateral strains together with uniaxial, equibiaxial or planar test data.

Additionally, the fabric layer has very low compressibility compared to its shear flexibility, and for this reason, the hyperelastic material model was also adopted for the fabric layer.

The most suitable mathematical model is the Ogden form. A strain energy potential is constructed that will reproduce the test data exactly and that will have reasonable behavior in other deformation modes.

The form of the Ogden strain energy potential is:

$$U = \sum_{i=1}^N \frac{2\mu_i}{\alpha_i^2} \left(\bar{\lambda}_1^{\alpha_i} + \bar{\lambda}_2^{\alpha_i} + \bar{\lambda}_3^{\alpha_i} - 3 \right) + \sum_{i=1}^N \frac{1}{D_i} \left(J^{el} - 1 \right)^{2i} \tag{8}$$

where $\bar{\lambda}_i$ is the deviatoric principal stretch $\bar{\lambda}_i = J^{-\frac{1}{3}} \lambda_i$; λ_i is the principal stretch; N is a material parameter; and μ_i , α_i and D_i are temperature-dependent material parameters. The initial shear modulus and bulk modulus for the Ogden form are given by:

$$\mu_0 = \sum_{i=1}^N \mu_i, K_0 = \frac{2}{D_1} \quad (9)$$

Since the fabric layer is stiffer and stronger than the rubber layer, its behavior is predominant, and for this reason, the Ogden material model was used to reproduce the structural behavior of the tank skin.

3.4. Tank Material Properties

The tank structure is made in a composite material that has a fabric nylon layer and an inner rubber layer aimed at ensuring impermeability to the fuel. Generally, the rubber layer is co-cured on the fabric layer, and the connection is very strong; possible failures involve both layers. The global response of the tank material can be related to a hyperplastic material, and therefore, a suitable material model was adopted in both Abaqus and Ls-Dyna. The best approach to defining the structural behavior is by means of obtaining the experimental stress–strain curve in a uniaxial tensile test. The density of the woven material is 1150 kg/m^3 , and the average thickness of the woven material is 2 mm. The stress–strain curve of the woven material, used as input, is reported in Figure 5.

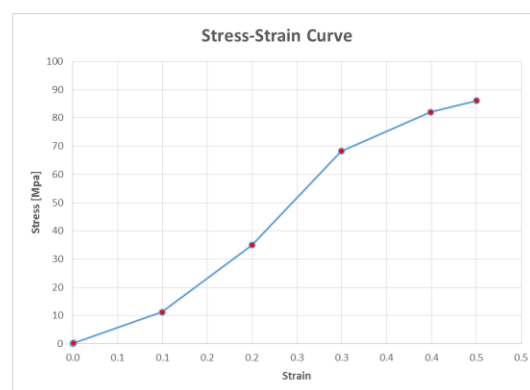


Figure 5. Stress–strain curve of the woven material.

4. Numerical Results

In the following, the comparison between Ls-Dyna and Abaqus results is shown. Figure 6 shows the deformed shape of the fuel tank in terms of global displacement (vectorial sum) for several time steps in order to provide a sort of deformation time-history.

The next figure shows that, generally, the two models behave quite similarly to each other. In particular, since the structure is very flexible, it begins to deform and is crushed in the lower area (the one that first comes into contact with the rigid ground). The internal fluid, under the action of inertial forces, pushes the tank structure downwards, introducing a moderate deformation state to the upper part. The magnitude of the global displacement is comparable between the two models, and therefore, the overall deformation of the structure does not present striking differences. However, it is equally evident that the structural response starts to exhibit some differences at around 40 ms. In fact, the Abaqus model seems to be softer, and therefore, the upper central part is subject to greater displacements. This is explained by the fact that the liquid begins to press towards the lateral walls in the bottom region (see also the following figures that report a sectional view). The fluid then generates an empty region that is unable to support the tank structure, and therefore, it collapses. On the other hand, in the LS-Dyna model, this peculiarity is not evident, and this is associated with the greater rigidity of the structure, which is therefore unable to accommodate fluid dislocations.

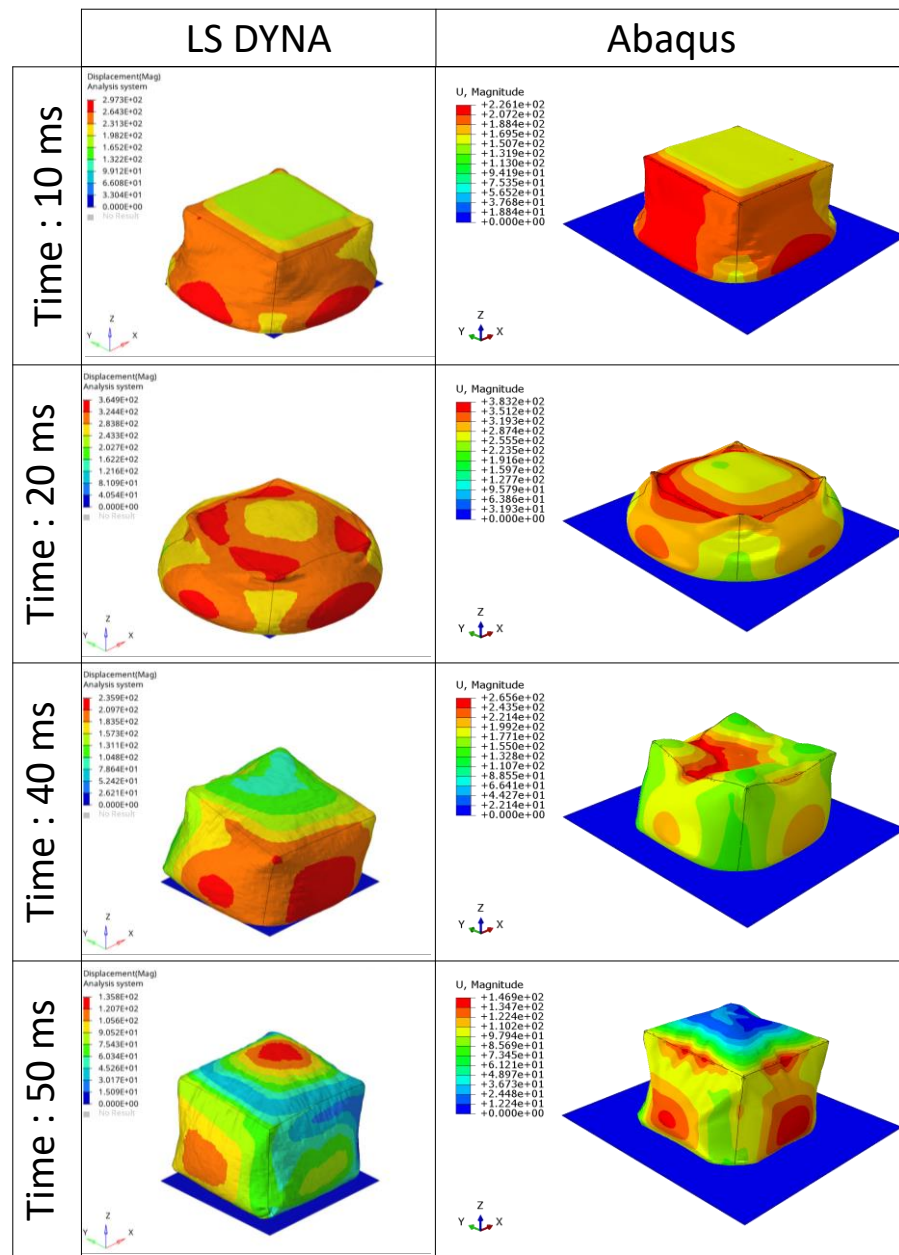


Figure 6. Global displacement contour plot. Left: Ls-Dyna model; right: Abaqus model.

Figure 7 shows the time histories of the strain of the bladder fuel tank for both the Ls-Dyna and Abaqus models. The distribution of the strain is quite different between the two models, even if, in terms of absolute values, they are still comparable. The biggest differences occur after the rebound stage. At 20 ms, the LS-Dyna model has a wide band with fairly high strain values (about 38%), so the area subject to high stretching is quite extensive. In the Abaqus model, on the other hand, only the areas close to the vertical edges show high strain values (around 32%). It is reasonable to assume that the largest strain values should be concentrated just in these areas, because the structure will try to eliminate the existing bends in order to accommodate fluid sloshing. The parts far from the edges, on the other hand, will be subject almost exclusively to a tensile stress state.

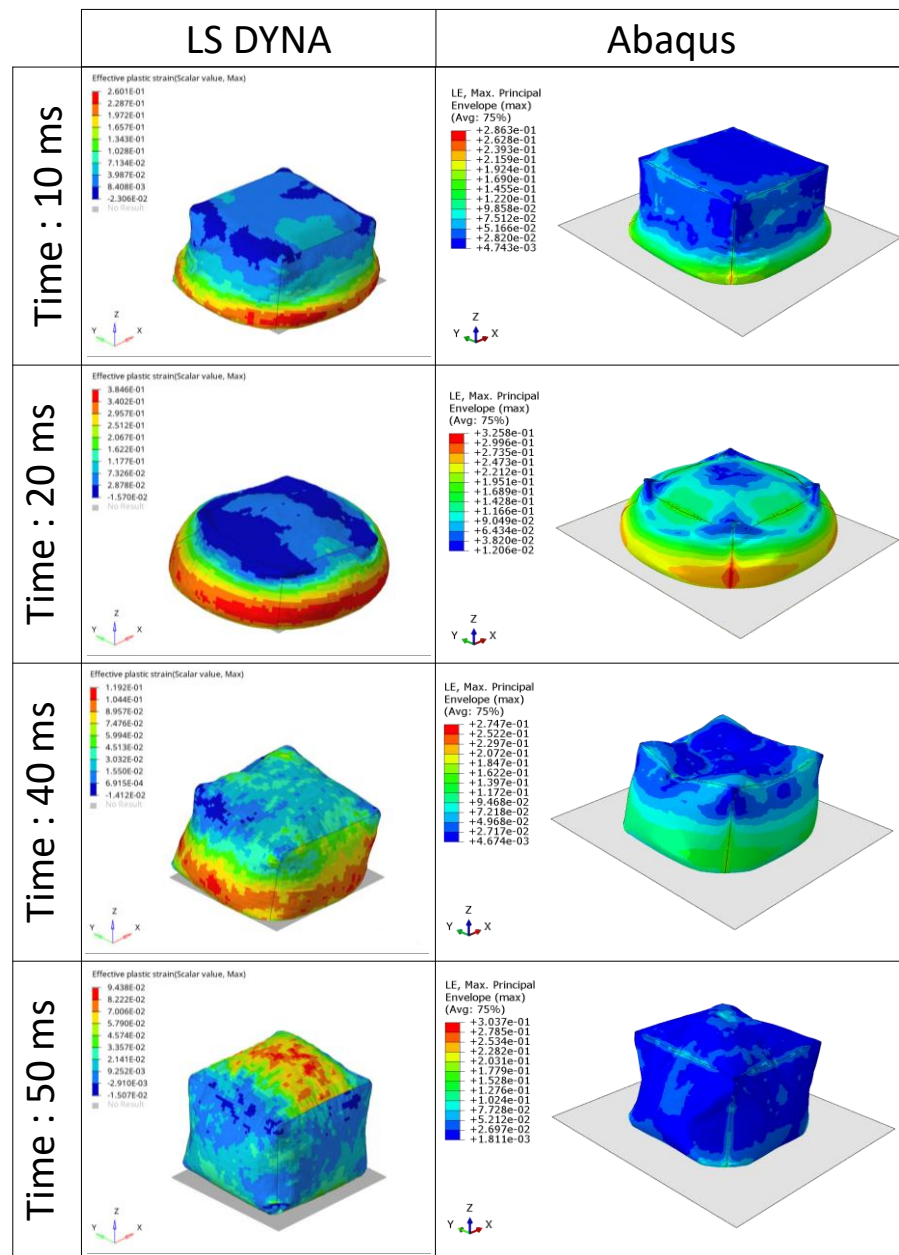


Figure 7. Strain distribution on tank structure. Left: Ls-Dyna model; right: Abaqus model.

After the rebound, at 40 ms, in the Ls-Dyna model, a wide region with high strain values remains (obviously, the values are smaller than those related to the maximum crushing step). On the other hand, in the Abaqus model, the regions with high strain values are always very reduced and localized in the bending areas. However, it should be noted that at 40 ms, the deformation state of the bottom regions presents comparable values between the two models (about 12% for Ls-Dyna and 14% for Abaqus). The top of the Ls-Dyna structure has an average strain state of about 4%, while in Abaqus, this area is not notably stressed since the average strain is about 0.4%. All of this, again, highlights the greater flexibility of the Abaqus model compared to the Ls-Dyna model.

Finally, at 50 ms, although the colors could be misleading, the maximum values on the top are comparable and are equal to about 10%. This is due to the fluid, which, after the rebound, is concentrated towards the area with minimum resistance, i.e., the central area, and pushes the tank from the inside upwards.

Figure 8 shows a section of the tank in which it is possible to see the global displacement of the SPH elements. The sectional view provides a clear overview of the behavior of the fluid inside the tank. Prior to 20 ms, there are no significant differences between the two models, as observed in the previous results. Even in this case, the greatest differences occur after the rebound phase. The Abaqus model allows for greater mobility of fluid particles, and thus, the sloshing is much greater. In fact, it is possible to note a clear mixing of the particles. Further, the 50 ms frame can explain the strain distribution on the top region. In Abaqus, the particles are more able to concentrate towards the central region, and therefore, in this area, the pressure is much greater. It is equally important to note that both models are able to accurately simulate the fluid–structure interaction. The particles remain contained within the tank and are able to slide easily on the internal walls. For example, at 10 ms, it is evident that there are large tank portions in which the fluid is not in direct contact with the structure.

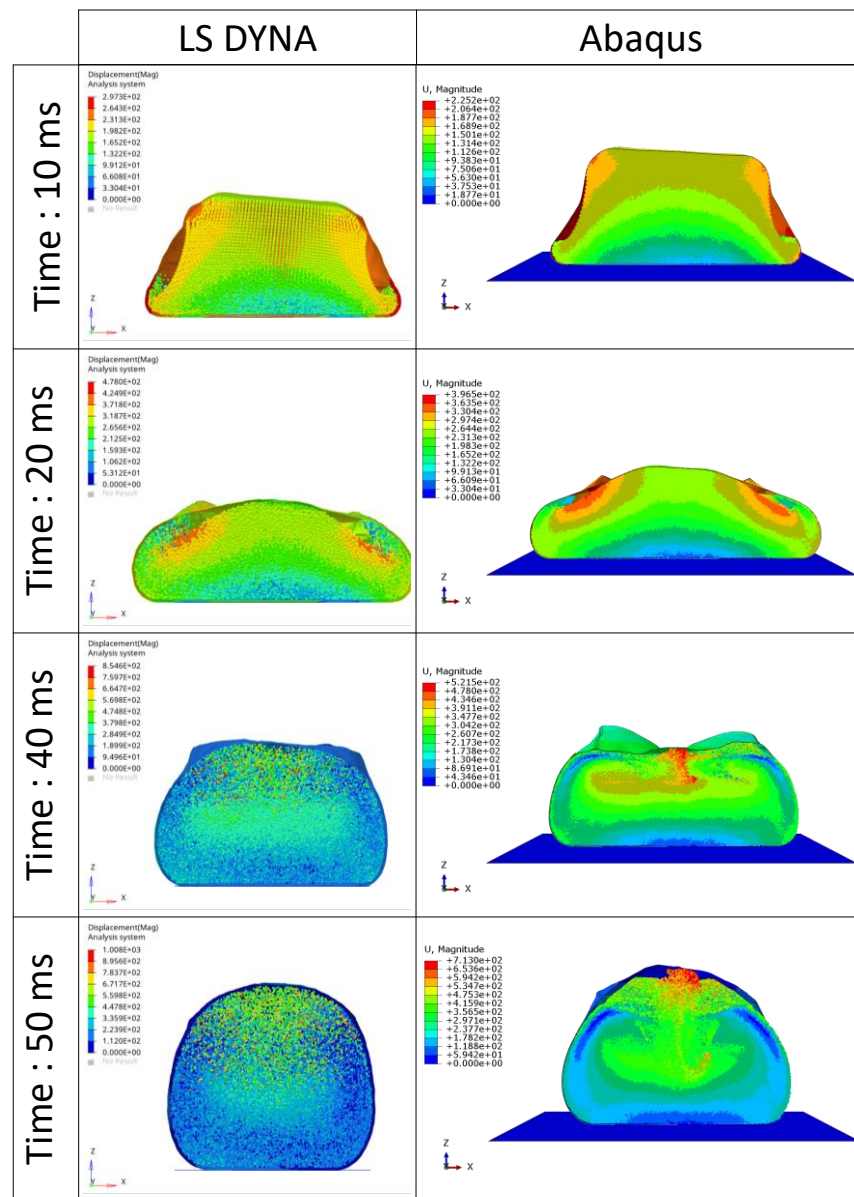


Figure 8. SPH global displacement field. Left: Ls-Dyna model; right: Abaqus model.

The force time–history curve (Figure 9) provides a global depiction of the good correlation level achieved by both models. The whole phenomenon is dominated by two force peaks, which are related to the first contact time and to the maximum crushing time. In

reference to this, the Abaqus model is more accurate since the Ls-Dyna model estimates the presence of a third peak (although with a reduced value). This could be related to the lower liquid fluidity (less sloshing), which leads to the concentration of inertial forces in more than two events. In addition, the overestimation of the second force peak by the LS-Dyna model could be related to the fact that the greater force is due to greater mass (therefore, more fluid is concentrated in the contact region due to a lower mobility capability and therefore a decreased ability to spread itself over a larger surface).

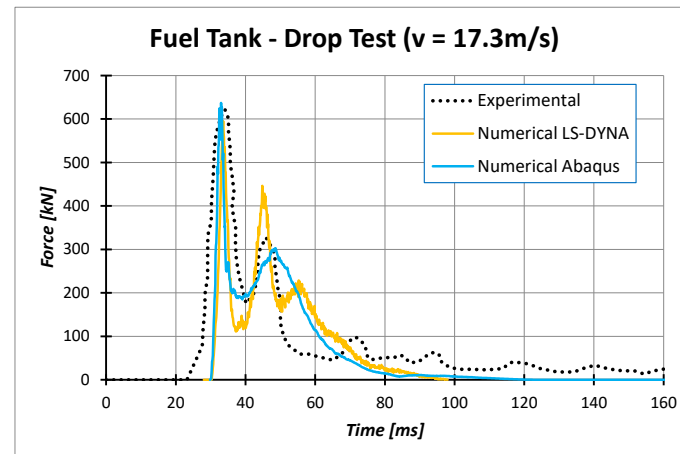


Figure 9. Numerical–experimental comparison in terms of impact force time-history.

In particular, the first experimental impact load peak is about 622 kN, whereas the value determined from the Abaqus model is 637.15 kN (+2.40%), and the value related to the Ls-Dyna model is 595.29 kN (−4.33%). As said before, the second force peak is well estimated by the Abaqus model since the error is about −7.45%, and it is quite overestimated by the Ls-Dyna model, which has an error of about +36%. Finally, both models overestimate the contact time by about 10 ms.

Another aspect to underline is that the experimental results do not show zero force after the rebound (an event that should occur at around 60 ms). This could be due to a poor damping capacity of the impact surface, since such structures are subject to significant rebounds if no catastrophic failures occur. Therefore, the comparison after that time step is not realistic.

5. Conclusions

This paper provides a comparison between two numerical models developed by means of two different explicit FE codes: Abaqus and LS-Dyna. The quality of the numerical results was verified by numerical–experimental comparison with respect to experimental data available in the literature related to the standard cube drop test for fuel tank certification.

- Having reliable and robust numerical models is a key factor in both realizing a good design and reducing the costs related to product certification. In fact, this research activity is motivated by the need to define numerical models applicable to the design and verification phases of the fuel storage system of the NGCRT-TD. In order to perform a fair comparison, the developed models have the same peculiarities; therefore, both simulate the tank structure by means of shell elements and a hyperelastic material model, and both models use the SPH approach for modeling the fluid. In particular, the most suitable mathematical formulation for the tank structure is the Ogden model. The material calibration curve was established using experimental tensile test data on samples consisting of a nylon layer and a rubber layer (the latter is essentially introduced to ensure the sealing capability).
- The results show that both codes are able to achieve an excellent correlation level with comparable computation costs. For both models, the error related to the maximum

impact force is smaller than 5% (a slightly better result was obtained with the Abaqus model). Both codes overestimate the duration of the main crash event (i.e., up to the rebound) to a similar extent. More significant differences can be found regarding the second peak of the impact force (relative to the instant of maximum crushing). In this case, Abaqus is clearly more accurate since the second peak is estimated with an error of about 7%.

- Regarding the structural response of the tank, the Abaqus model is able to simulate greater flexibility. This allows both better accommodation of the movements of the internal fluid and therefore a more realistic deformation mode, and it provides a strain distribution with reduced average values localized in a few regions, such as the edges.
- Finally, as regards the dynamics of the fluid particles, minimal differences are found up to the maximum crushing time, but after that, the differences are more significant. The Abaqus model is able to simulate a high state of particle mixing, and therefore, the resulting sloshing is more extensive and more realistic. It would be interesting to experimentally study the real degree of sloshing in such crash events. This is, obviously, a key aspect since, due to the high material flexibility, the fluid is able to stretch the tank structure with its pressure.

Author Contributions: Conceptualization, D.C., F.D.C., C.P. (Claudio Pezzella), C.P. (Carmen Paciello), S.M. and M.B.; methodology, D.C., F.D.C., C.P. (Claudio Pezzella) and C.P. (Carmen Paciello); validation, D.C., C.P. (Carmen Paciello) and S.M.; formal analysis, D.C. and C.P. (Carmen Paciello); data curation, D.C., F.D.C. and S.M.; writing—original draft preparation, D.C., F.D.C., C.P. (Claudio Pezzella), C.P. (Carmen Paciello), S.M. and M.B; writing—review and editing, F.D.C.; funding acquisition L.D.P.; supervision, L.D.P. All authors have read and agreed to the published version of the manuscript.

Funding: This research was funded by the Clean Sky 2 Joint Undertaking under the European Union’s Horizon 2020 research and innovation program, Grant Agreement number: 738078—DEsign, development, manufacture, testing and Flight qualification of nExt geNeration fuel storage system with aDvanced intEgRated gauging and self-sealing capabilities (DEFENDER).

Institutional Review Board Statement: Not applicable.

Informed Consent Statement: Not applicable.

Data Availability Statement: Not applicable.

Conflicts of Interest: The authors declare no conflict of interest.

References

1. Sillers, P. T-WING: In Conversation with CIRA. Available online: <https://www.cleansky.eu/clean-skys-t-wing-in-conversation-with-cira> (accessed on 28 January 2022).
2. Perry, D. ANALYSIS: Leonardo Helicopters Advances on Next-Gen Tiltrotor. Available online: <https://www.flightglobal.com/analysis/analysis-leonardo-helicopters-advances-on-next-gen-tiltrotor/131350.article> (accessed on 28 January 2022).
3. European Aviation Safety Agency. “Certification Specifications for Large Rotorcraft—CS-29”, Amendment 10. December 2021. Available online: <https://www.easa.europa.eu/document-library/certification-specifications/cs-29-amendment-10> (accessed on 10 March 2022).
4. Belardo, M.; Marano, A.D.; Beretta, J.; Diodati, G.; Graziano, M.; Capasso, M.; Di Palma, L. Wing Structure of the Next-Generation Civil Tiltrotor: From Concept to Preliminary Design. *Aerospace* **2021**, *8*, 102. [CrossRef]
5. Freudenruch, C. How the V-22 Osprey Works. HowStuffWorks. Available online: <https://science.howstuffworks.com/osprey.html> (accessed on 28 January 2022).
6. Cronkhite, J.D.; Tanner, A.E. Tilt Rotor Crashworthiness. In Proceedings of the 41st American Helicopter Society (AHS) Forum, Ft. Worth, TX, USA, 15–17 May 1985. Available online: <https://vtol.org/store/product/tilt-rotor-crashworthiness-1489.cfm> (accessed on 28 January 2022).
7. Di Palma, L.; Di Caprio, F.; Chiariello, A.; Ignarra, M.; Russo, S.; Riccio, A.; De Luca, A.; Caputo, F. Vertical Drop Test of Composite Fuselage Section of a Regional Aircraft. *AIAA J.* **2020**, *58*, 474–487. [CrossRef]
8. Perfetto, D.; Lamanna, G.; Manzo, M.; Chiariello, A.; di Caprio, F.; di Palma, L. Numerical and Experimental Investigation on the Energy Absorption Capability of a Full-Scale Composite Fuselage Section. *Key Eng. Mater.* **2019**, *827*, 19–24. [CrossRef]
9. Riccio, A.; Saputo, S.; Sellitto, A.; Russo, A.; Di Caprio, F.; Di Palma, L. An Insight on the Crashworthiness Behavior of a Full-Scale Composite Fuselage Section at Different Impact Angles. *Aerospace* **2019**, *6*, 72. [CrossRef]

10. Riccio, A.; Saputo, S.; Sellitto, A.; Di Caprio, F.; di Palma, L. A numerical-experimental assessment on a composite fuselage barrel vertical drop test: Induced damage onset and evolution. *Compos. Struct.* **2020**, *248*, 112519. [[CrossRef](#)]
11. Caputo, F.; Lamanna, G.; Perfetto, D.; Chiariello, A.; Di Caprio, F.; Di Palma, L. An experimental and numerical crash-worthiness study of a full-scale composite fuselage section. *Aeronaut. Astronaut.* **2020**, *59*, 685–703. [[CrossRef](#)]
12. Giavotto, V.; Caprile, C.; Sala, G. The design of helicopter crashworthiness. Energy absorption of aircraft structures as an aspect of crashworthiness. In Proceedings of the AGARD 66th Meeting of the Structures and Material Panel, Luxembourg, 1–6 May 1988; pp. 6.1–6.9.
13. Paciello, C.S.; Pezzella, C.; Belardo, M.; Magistro, S.; Di Caprio, F.; Musella, V.; Lamanna, G.; Di Palma, L. Crashworthiness of a Composite Bladder Fuel Tank for a Tiltrotor Aircraft. *J. Compos. Sci.* **2021**, *5*, 285. [[CrossRef](#)]
14. Harris, F.D.; Kasper, E.F.; Iseler, L.E. US Civil Rotorcraft Accidents, 1963 through 1997. NASA STI Program, NASA/TM-2000-209597, USAAMCOM-TR-00-A-006. 2000. Available online: <https://citeseeerx.ist.psu.edu/viewdoc/download?doi=10.1.1.976.8762&rep=rep1&type=pdf> (accessed on 28 January 2022).
15. Robertson, S.H.; Johnson, N.B.; Hall, D.S. *A Study of Transport Airplane Crash-Resistant Fuel Systems*; Robertson Aviation LLC: Tempe, AZ, USA, 2002.
16. Anghileri, M. Crash behavior of helicopter fuel tank structures. *US Army* **1998**, *64*, 95–159.
17. Anghileri, M.; Castelletti, L.-M.; Tirelli, M. Fluid–structure interaction of water filled tanks during the impact with the ground. *Int. J. Impact Eng.* **2005**, *31*, 235–254. [[CrossRef](#)]
18. Li, Z.; Jin, X.L.; Chen, X.D. The simulation of dual layer fuel tank during the impact with the ground based on parallel computing. *J. Comput. Nonlinear Dyn.* **2007**, *2*, 366–373.
19. Luo, C.; Liu, H.; Yang, J.-L.; Liu, K.-X. Simulation and Analysis of Crashworthiness of Fuel Tank for Helicopters. *Chin. J. Aeronaut.* **2007**, *20*, 230–235. [[CrossRef](#)]
20. Kim, H.-G.; Kim, S. Numerical simulation of crash impact test for fuel cell group of rotorcraft. *Int. J. Crashworthiness* **2014**, *19*, 639–652. [[CrossRef](#)]
21. Wang, Y.; Liew, J.R. Blast performance of water tank with energy absorbing support. *Thin-Walled Struct.* **2015**, *96*, 1–10. [[CrossRef](#)]
22. Wang, Y.; Liew, J.R.; Lee, S.C. Structural performance of water tank under static and dynamic pressure loading. *Int. J. Impact Eng.* **2015**, *85*, 110–123. [[CrossRef](#)]
23. Yang, X.; Zhang, Z.; Yang, J.; Sun, Y. Fluid–structure interaction analysis of the drop impact test for helicopter fuel tank. *SpringerPlus* **2016**, *5*, 1573. [[CrossRef](#)] [[PubMed](#)]
24. Monaghan, J.J.; Lattanzio, J.C. A refined particle method for astrophysical problems. *Astron. Astrophys.* **1985**, *149*, 135143.